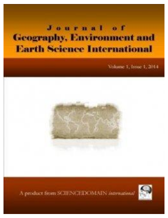

Journal of Geography, Environment and Earth Science International

15(1): 1-14, 2018; Article no.JGEESI.40930
ISSN: 2454-7352

Geochemical Characteristics of Metasomatised Diorites in and around Umsopri of Ri-bhoi District, Meghalaya, India

Anamika Gogoi[1] and Balen Bhagabaty[1*]

[1]*Department of Geological Sciences, Gauhati University, Guwahati-781014, Assam, India.*

Authors' contributions

This work was carried out in collaboration between both authors. Author AG designed the study, performed the statistical analysis, wrote the protocol, and wrote the first draft of the manuscript. Author BB managed the analyses of the study. Both authors read and approved the final manuscript.

Article Information

DOI: 10.9734/JGEESI/2018/40930
Editor(s):
(1) Iovine Giulio, CNR-IRPI (National Research Council-Institute of Research for the Geo-hydrologic Protection) of Cosenza, Italy.
Reviewers:
(1) Mustafa Kumral, Istanbul Technical University, Turkey.
(2) Adewumi Adeniyi JohnPaul, Achievers University, Nigeria.
Complete Peer review History: http://www.sciencedomain.org/review-history/24417

Original Research Article

Received 10th February 2018
Accepted 18th April 2018
Published 1st May 2018

ABSTRACT

The metasomatised dioritic rocks are well exposed in and around Umsopri area (N 25°49/ and E91°39/), Ri-Bhoi district of Meghalaya, along with granitoid rocks. The gneissic complex represents the basement of the Shillong plateau comprising a group of high-grade metamorphic rocks including basic granulite, amphibolite, quartzofeldspathic gneiss, migmatite, calc-silicate gneiss and garnet sillimanite-bearing metapelite. The basement rocks of the Shillong plateau is intruded by Neoproterozoic granitoids of multiple phases. The granitoids are younger in age from south-west to north-east. The Shillong Plateau along with Mikir Hills experienced four major phases of felsic magmatic episodes at ~1800 Ma, ~1600 Ma, ~1400 Ma, and ~500 Ma. Petrographicaly, the rock is composed of K-feldspar, plagioclase, hornblende, quartz along with accessory phases like sphene, apatite, zircon, rutile, ilmenite, etc. The metasomatic effect has been inferred by the formation of biotite and sphene at the expanse of Hornblende. The rocks have moderate SiO_2 content (52.55 to 55.84 wt%). Trace elements Rb, Ba, Nb shows a negative trend with SiO_2 concentrations. The high field strength elements like Nb, Zr, La, Th, U show a negative correlation and Y shows a positive correlation with an increase in abundance of SiO_2. Large ion lithophile

**Corresponding author: E-mail: b_bhagabaty@rediffmail.com;*

element Rb shows a negative correlation with SiO_2 while Sr shows a positive correlation with SiO_2. Geochemical features indicates that the rock is metaluminous in character and tectonically in the WPG (within plate granitoid) field.

Keywords: Shillong plateau; diorites; geochemistry; metasomatism.

1. INTRODUCTION

The Shillong Plateau of north-east India is a tectonically detached part of the Indian Peninsular shield. The oldest rocks of the plateau are represented by basement gneissic complex. It comprises a group of high-grade metamorphic rocks including basic granulite, amphibolite, quartzofeldspathic gneiss, migmatite, calc-silicate gneiss and garnet sillimanite-bearing metapelite [1]. The basement rocks of the Shillong plateau is intruded by Neoproterozoic granitoids of multiple phases [2,3]. South Khasi batholiths, Mylliem pluton, Kyrdem and Nongpoh batholiths are some significant granitoids of Meghalaya plateau. The granitoids are younger in age from south-west to north-east [4]. The ages of these granitoids are in the range from 479 to 881 Ma [4–12]. The Shillong Plateau along with Mikir Hills experienced four major phases of felsic magmatic episodes at ~1800 Ma (Rongjeng granite gneiss: 1778±37 Ma), ~1600 Ma (Sonsak granite gneiss: 1620.8±9.2 Ma), ~1400 Ma (Longavalli granite gneiss: 1430.4±9.6 Ma), and ~500 Ma (Kaziranga: 528.7±5.5 Ma; South Khasi: 516±9.0 Ma; Kyrdem: 512.5±8.7 Ma; Nongpoh: 506.7±7.1 Ma and 535±11 Ma) [13]. The present study has an attempt to first report of metasomatised dioritic rocks in and around Umsopri (N 25°49$^{/}$ and E91°39$^{/}$), Ri-Bhoi district of Meghalaya. The different rock units along with dioritic rocks are shown in Fig.1. This paper highlights the petrography and geochemical characteristics of metasomatised dioritic rocks of the Shillong Plateau.

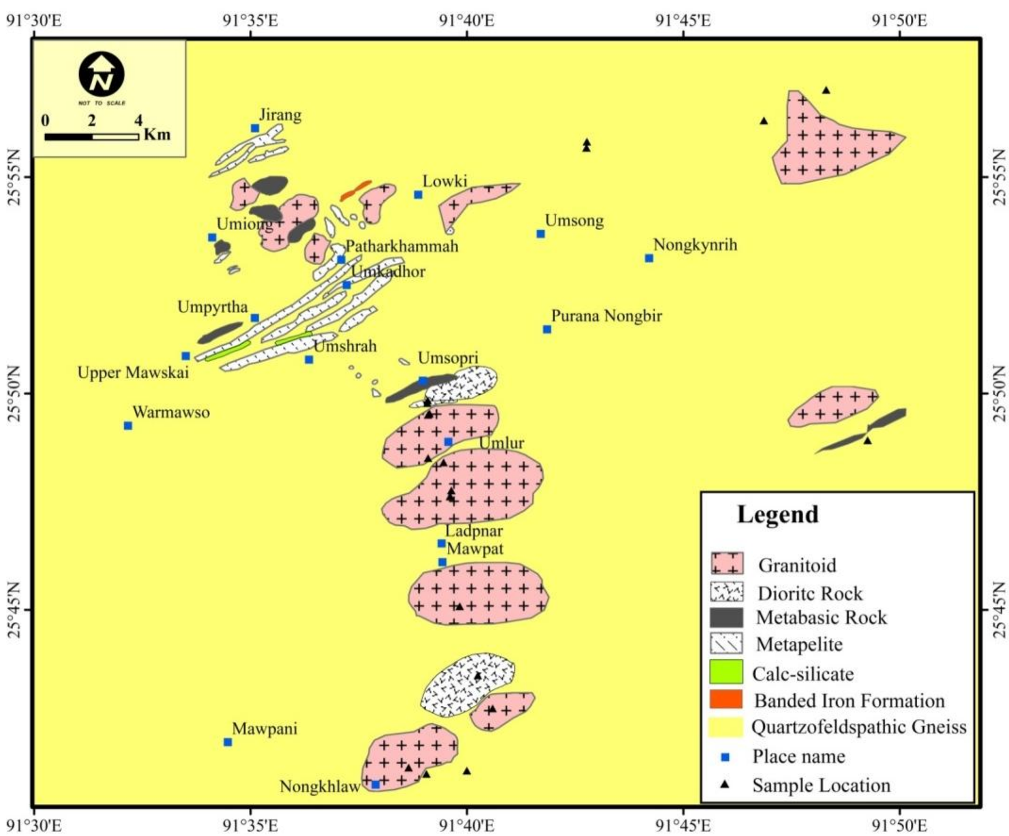

Fig. 1. Geological map of the study area

2. MATERIALS AND METHODS

The intrusive nature of the diorites is indicated by field evidence like cross-cut relation of the rocks with the country rocks. The rocks have sharp contact relationships with quartz-feldspathic gneiss and amphibolite (Figs. 2A & 2B). There is lots of feldspar bearing veins within the rocks (Fig. 2C & 2D). The rocks are mainly composed of K-feldspar, plagioclase, biotite, hornblende, quartz and accessory opaque oxides, sphene, apatite, chlorite, zircon, zoisite, rutile, etc. Plagioclase occurs mainly as the medium to coarse, tabular, subhedral grains. Biotite occurs as coarse to medium grains. Hornblende are yellowish green to brownish green to dark green in colour and occurs as the medium to coarse grains, commonly associated with biotite. In most of the samples, biotite appears to be formed at the expanse of hornblende due to the effect of metasomatism (Fig. 3A). This is inferred from the symplectitic intergrowth of sphene and biotite and also reflected from the negative correlation of modal hornblende and biotite (Fig. 3B).

Pseudomorphous replacement of hornblende is indicated by the presence of hornblende within biotite (Fig. 3C). Common occurrence of sphene is observed in most of the samples. Co-existence of biotite and hornblende and the absence of aluminosilicate like muscovite is one of the characteristic features of the rocks. Presence of hornblende domain without sphene and biotite domain with sphene has petrogenetic significance (Fig.3D). The co-existence of biotite and sphene has an indication that these are formed from the hornblende due to the effect of metasomatism.

Eight representative samples were analysed for major and trace elements including rare earth elements (REE)) at Wadia Institute of Himalayan Geology, Dehradun, India. Major elements were determined by X-ray fluorescence (XRF) analysis using instrument Siemens SRS-3000. Whereas trace elements including REE were determined using Inductively Coupled Plasma and Mass Spectrometry (ICP-MS) technique through Perkin Elmer SCIX ELAN DRC-E instrument.

3. RESULTS

3.1 Geochemical Characters

Geochemical study of the rocks is essential to classify and understand the origin and geodynamic environment of emplacement of those rocks. Various geochemical discrimination diagrams were used in the present study to classify and find out the origin and geodynamic environment of emplacement of these rocks.

Fig. 2. A. Contact between doritic rock and QFG; B. Contact between dioritic rock and amphibolites; C. Feldspar bearing vein within dioritic rock; D. Patches of feldspar bearing vein within dioritic rock

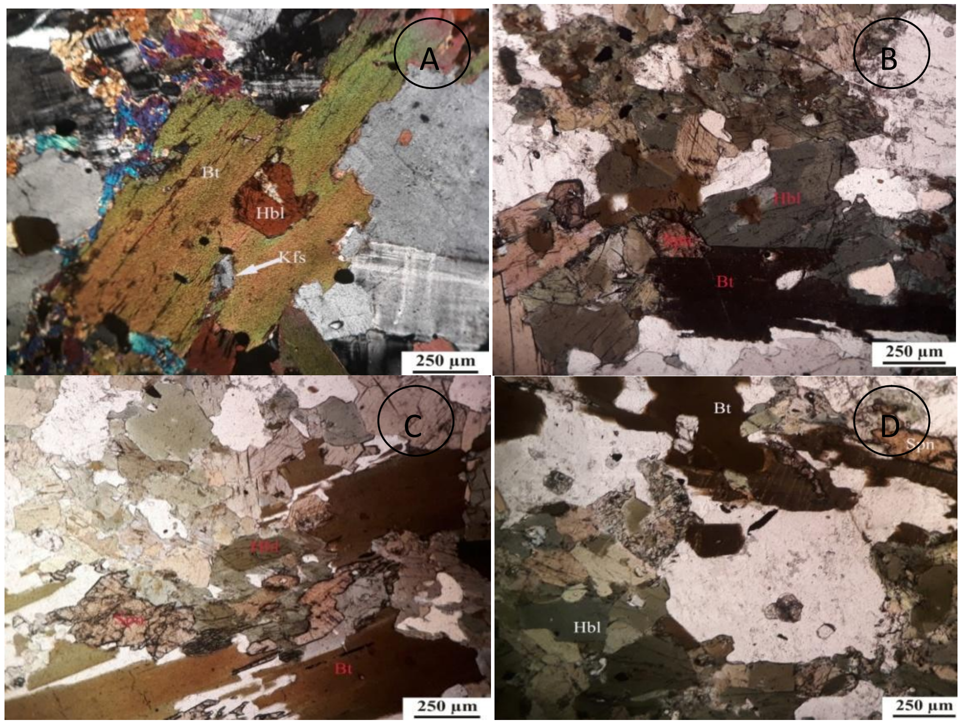

Fig. 3. A. Pseudomorphous replacement of hornblende by biotite; B. Growth of sphene at the border of biotite; C. Replacement of hornblende by biotite; D. Hornblende domain without sphene and biotite domain with cluster of sphene

Major element oxide data (Table 1) reveal that the rocks have moderate SiO_2 content (52.55 to 55.84 wt%), CaO (4.34 to 6.77 wt%), TiO_2 (1.1 to 1.53 wt%), MnO (0.11 to 0.16 wt%), P_2O_5 (0.55 to 0.92 wt%) and Al_2O_3 (12.71 to 14.27 wt%). Total alkali content ranges from 6.21 to 8.12 wt%. The K_2O/Na_2O ratio varies from 1.785 to 3.401 wt% indicating K rich characteristics of the diorites.

The trace element (including REE) analyses are given in Table 2 and ratios of specific trace elements are shown in Table 3. Among the trace elements Rb, Ba, Nb shows a negative trend with SiO_2 concentrations. The high field strength elements (HFSE) like Nb, Zr, La, Th, U show a negative correlation and Y shows a positive correlation with increase in abundance of SiO_2. Large ion lithophile (LIL) element Rb shows a negative correlation with SiO_2 while Sr shows a positive correlation with SiO_2. Trace element data show variable Th/U ratios (vary from 4.559 to 7.484) indicating a relatively higher abundance of Thorium over Uranium. Sr increases with increase in Ba. Zr shows a positive co-relation with Y. Y/Nb (varies from 0.9 to 1.7, average 1.2), La/Nb (varies from 1.9 to 3.1, average 2.4) and Rb/Sr (varies from 0.13-0.24, average 0.24) are low. The concentrations of Cu (avg. 29 ppm), V (avg.169 ppm), Cr (avg. 387 ppm), Sr (avg.733 ppm) and $(La/Yb)_N$ are high (avg. 13.028). $(Ce/Yb)_N$ shows a range of 6.588 to 12.744. $(Ho/Yb)_N$ varies less (0.106 t0 0.122).

The rocks are enriched in light rare earth element (LREE) relative to heavy rare earth element (HREE) (Table 2,). Chondrite normalised plot indicates a predominance of LREE over HREE, steeper slopes from La to Sm, relatively flat pattern from Gd to Lu and negative Eu anomalies. Chondrite normalised spider diagram for incompatible trace element pattern shows prominent depletion of Nb, Sr, Ti and P. The rocks plot in the Quartz monzonite field in normative An-Ab-Or plot (Fig. 4) [14]. The rocks plot in monzonite and Monzo-diorite field in the total alkali silica (TAS) diagram of Middlemost (1985) [15] has been presented in Fig. 5. In the TAS diagram MacDonald (1968) indicated the alkaline nature of these rocks (Fig. 6) [16]. The $Al_2O_3/(CaO+Na_2O+K_2O)$ [A/CNK] and $Al_2O_3/(Na_2O+K_2O)$ [A/NK] plot indicated the metaluminous nature of the rocks (Shand, 1943) (Fig. 7) [17].

4. DISCUSSION

Trace elements Ni, Cr, Sc, V, Rb, Ba, Sr, Zr, Y, Nb and REE (La to Lu) are significant in interpretation of petrogenesis of the rocks. $(La/Yb)_N$ is high (avg. 13.028). La/Yb is used as an index of fractionation of LREE from HREE [18]. The REE data for studied rocks shows an abundance of LREE and relatively low HREE. The negative Eu anomaly in chondrite normalised REE pattern is due to fractionation of plagioclase (Fig. 8) [19]. The $(Tb/Yb)_N$ >1 in the rocks indicates a high degree of HREE fractionation. The $(La/Sm)_N$ (avg. 3.492), $(La/Yb)_N$ (avg.13.028) and $(Ce/Yb)_N$ (avg. 10.797) are indicative of higher levels of fractionation and differentiation. The similar type of REE pattern is also observed in many Pan-African granitoids [12].

The Eu/Eu* in the diorite (0.649 to 0.783, avg. 0.723) is indicative of high fO_2 of crystallising magma [18]. The Eu anomaly (Eu/Eu* ranging from 0.649 to 0.783) is indicting a significant role of plagioclase fractionation from the parent magma. Abundance of LREE +Y and relatively low HREE indicate partial melting of lower crust producing calc alkaline melt [20]. $(Ce/Yb)_N$ values show a range of 6.588 to 12.744 which indicates a strong REE element fractionation. $(Ho/Yb)_N$ varies less (0.106 to 0.122) indicating mild HREE fractionation. The Sr and Eu depletion (Fig. 8,9) indicates small degrees of partial melting of mantle rock at shallow depth, and fractionation of plagioclase causing depletion of Sr and Eu [21]. The Eu anomaly (Eu/Eu* ranging from 0.649 to 0.783, avg. 0.723) indicates a significant role of plagioclase fractionation from the parent magma. The strong negative Eu anomaly of these rocks may be due to the removal of plagioclases from the melt composition [22]. They exhibit variations in total REE content (∑REE = 277.4 - 482.33 ppm) and also exhibit clear crystal fractionation trend regarding both the LREE (avg. La_N/Sm_N = 5.611) and avg. Gd_N/Yb_N = 2.263). In the Rb-(Y+Nb) diagram the rocks are plotted in WPG (Within Plate Granitoid) field (Fig. 10) [23]. There are two principal causes of intraplate magma generation: i) mantle plume activity and (ii) passive rifting. In the former, mantle plumes impact upon the base of the continental or oceanic lithosphere. In the later, lithospheric extension causes sufficient decompression for the mantle to melt. In some cases, the two mechanisms can act together and here the greatest volume of magma is likely to be generated [24]. The WPG has geochemical features that reflect enriched mantle sources and anhydrous crystallisation with variable interaction with continental crust [25]. The Nb has depleted in the source and thus crustal contamination can be taken into consideration. The increased value of the Zn contents (84 –116 ppm) also reflects the signature of crustal contamination.

Feldspar triangle (O'Connor 1965)

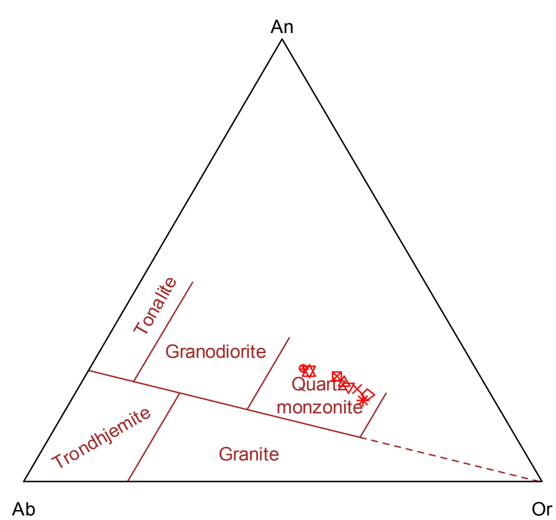

Fig. 4. Ab-An-Or plot (after O'Connor, 1965) indicating quartz-monzonite fields for the rocks

These diorites occur in both pre and post-collisional tectonic settings (Fig. 11) [26]. It is also related to subsequent post closure of anorogenic belt. Post-collisional diorites can be resulted from melting of the lower crust by thermal relaxation after collision. The present rocks (metasomatised diorites) fall in the A- type and also in the I&S type field in Ga discrimination diagram (Fig.12) [27]. A- type granitoids can be formed by two petrogenetic schemes like differentiation of basaltic magma and melting of lower continental crust. In the first case interaction with crustal material modifies the chemistry of the initial magma. Anorogenic granitoids contain high SiO_2 up to 77% but the present rocks contain an intermediate range of SiO_2. The high Th/U concentration due to U depletion is an indication of involvement of lower crustal gabbroic component in the generation of diorites.

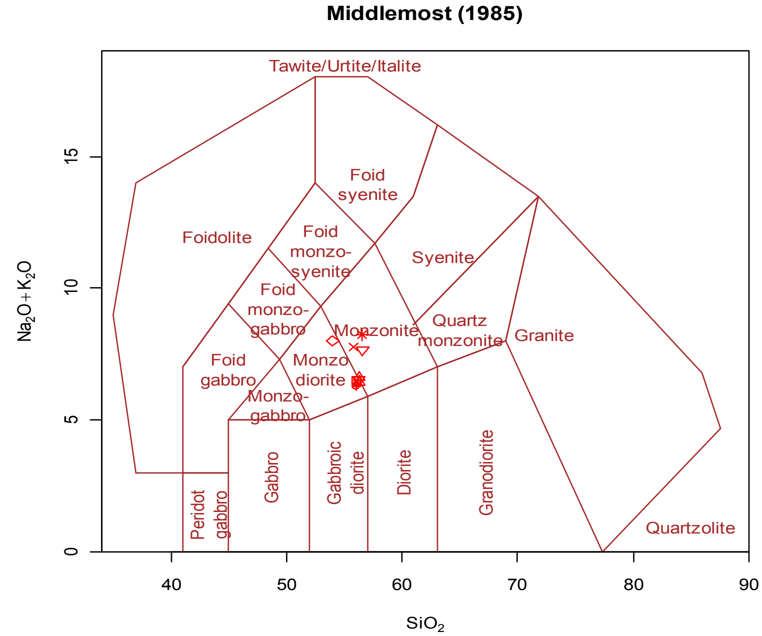

Fig. 5. The SiO_2 - (Na_2O + K_2O) wt% plot (after Middlemost, 1985) indicating monzonite and monzo-diorite fields

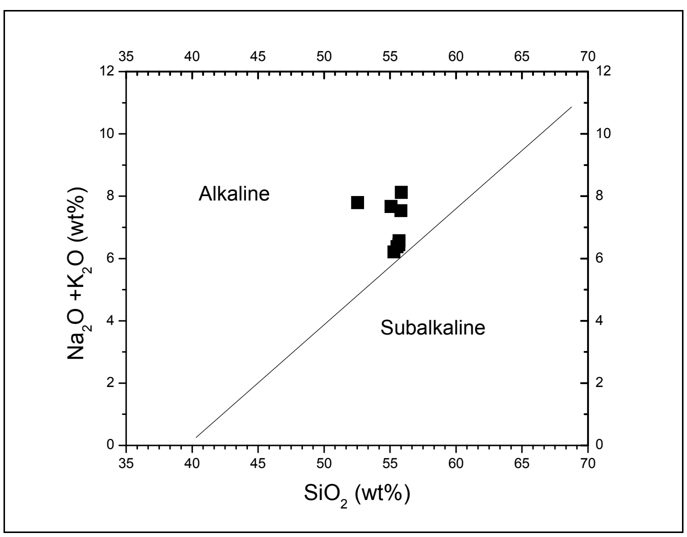

Fig. 6. TAS plots (after MacDonald, 1968) showing alkaline nature of the rocks

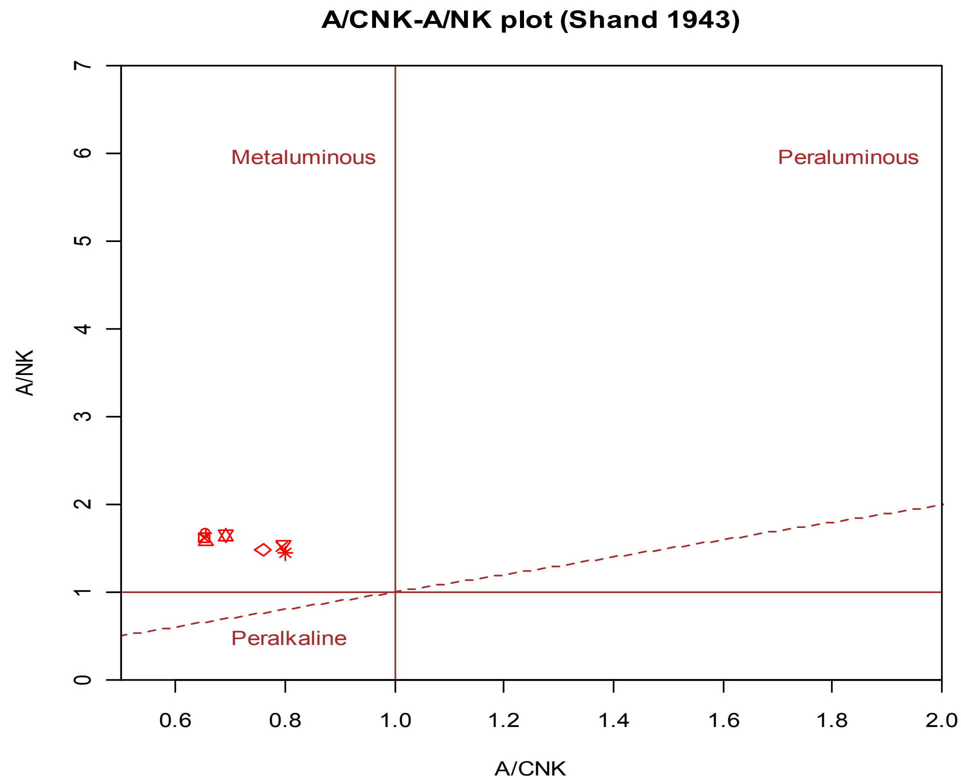

Fig. 7. Metaluminous nature of rocks indicated by A/CNK vs A/NK plot (after Shand, 1943)

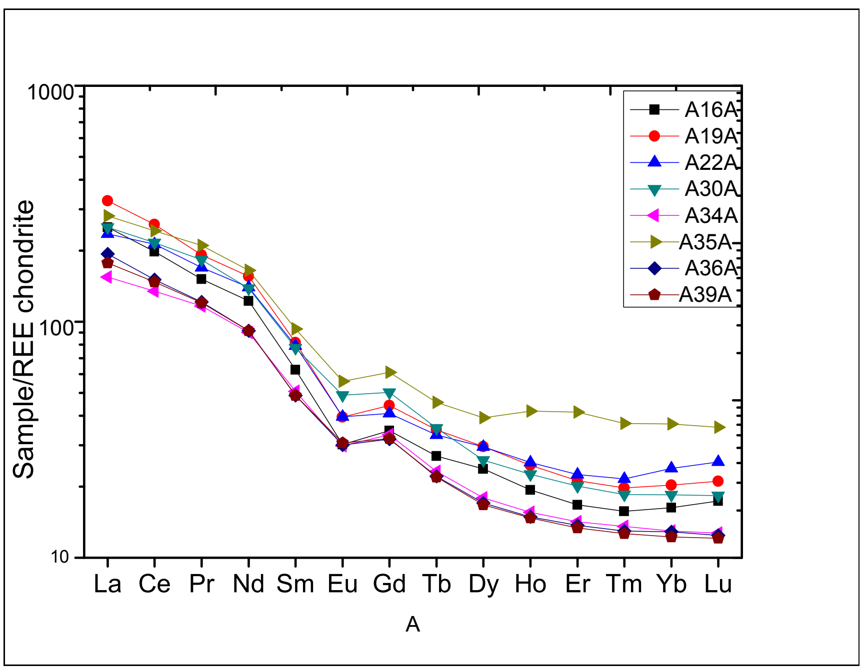

Fig. 8. Chondrite-normalised REE plot (after Boynton, 1984) showing relatively less abundance of HREE for diorite rocks. REE: Rare Earth Element; HREE: Heavy Rare Earth Element

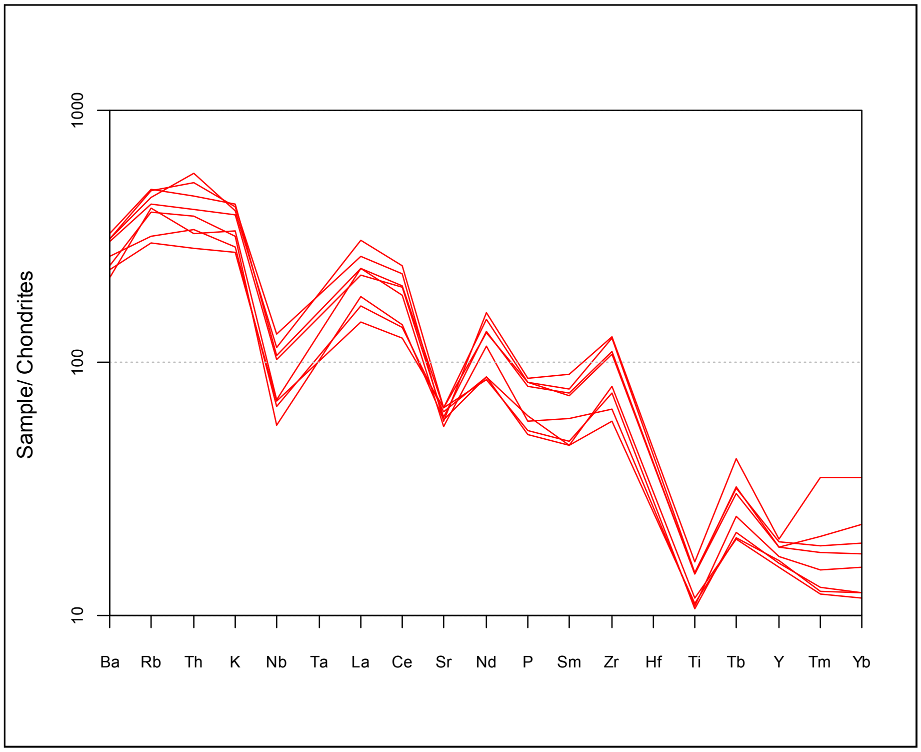

Fig. 9. Chondrite – normalised spider plot (after Thompson, 1984) showing prominent depletion of Nb, Sr and Ti in all 08 diorite rocks

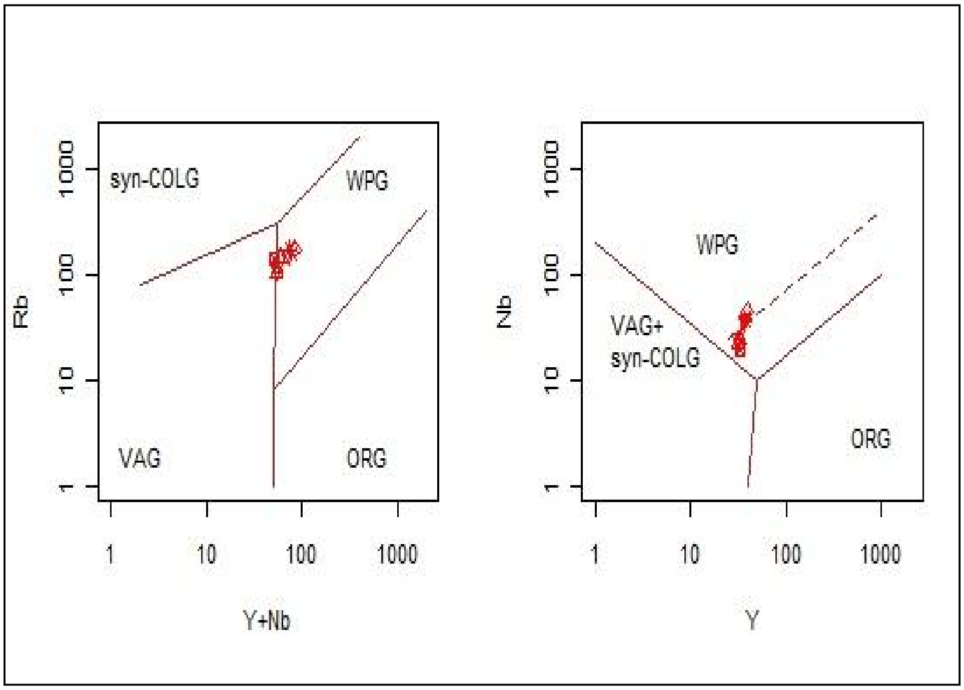

Fig. 10. The (Y + Nb) vs. Rb, Y vs. Nb, plots (after Pearce et al., 1984) showing within plate granitoid (WPG) fields for dioritic rocks

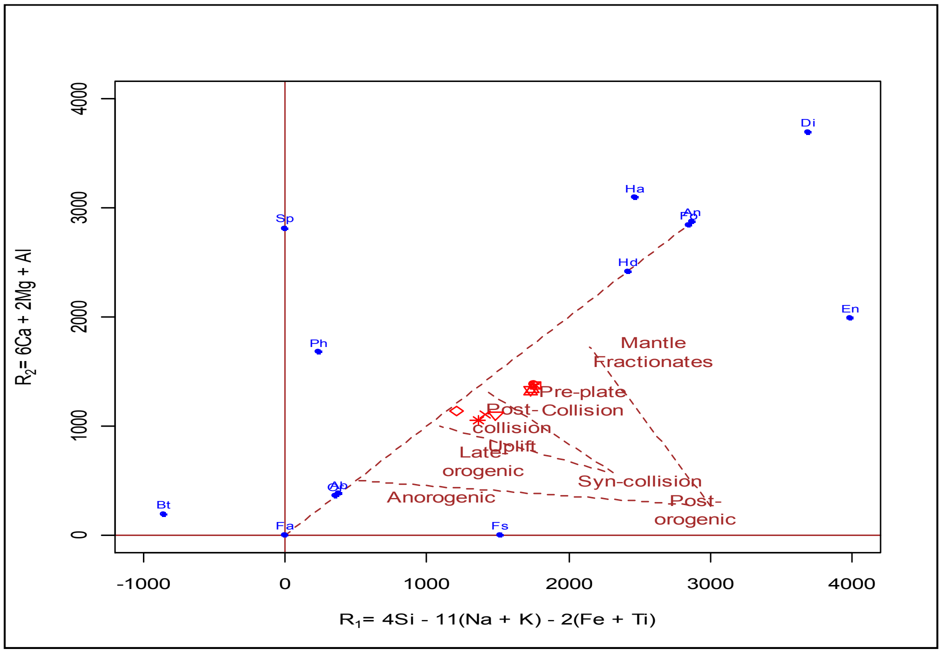

Fig. 11. R1 vs. R2 diagram (after Batchelor and Bowden, 1985) showing pre-plate collision to post-collision tectonic settings of dioritic rocks

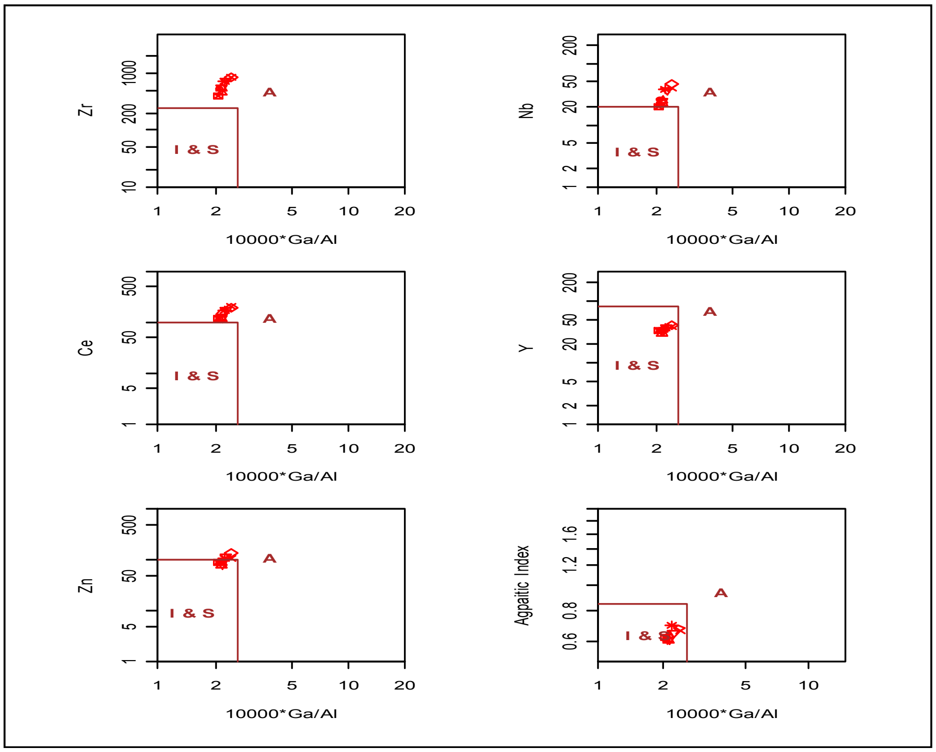

Fig. 12. The (10000 * Ga/Al) vs. Zr, (10000 * Ga/Al) vs. Nb, (10000 * Ga/Al) vs. Ce, (10000 * Ga/Al) vs. Y, (10000 * Ga/Al) vs. Zn and (10000 * Ga/Al) vs. Agpaitic Index plots (after Whalen et. al., 1987) clearly indicating A-type fields for the dioritic rocks

Table 1. Major element oxide data of dioritic rocks

	A16A	A19A	A22A	A30A	A34A	A35A	A36A	A39A
SiO_2	55.7	55.09	55.84	55.86	55.31	52.55	55.68	55.54
TiO_2	1.12	1.53	1.5	1.51	1.1	1.68	1.15	1.21
Al_2O_3	12.71	14.2	14.27	14.22	13.27	13.96	12.91	13.43
Fe_2O_3	7.46	7.89	7.55	7.53	7.32	8.58	7.29	7.09
MnO	0.12	0.12	0.14	0.11	0.12	0.16	0.13	0.11
MgO	8.54	6.68	6.24	6.18	8.11	6.77	8.65	8.01
CaO	6.2	4.68	4.76	4.34	6.77	4.93	6.47	6.21
Na_2O	1.78	1.89	1.99	1.94	2.23	1.77	1.84	2.22
K_2O	4.79	5.78	5.55	6.18	3.98	6.02	4.6	4.16
P_2O_5	0.62	0.88	0.85	0.88	0.57	0.92	0.55	0.65
LOI	0.93	1.01	0.95	0.91	1	1.02	1.03	1.11
Total	99.97	99.75	99.64	99.66	99.78	98.36	100.3	99.74
Na_2O+K_2O	6.57	7.67	7.54	8.12	6.21	7.79	6.44	6.38
A/CNK	0.66	0.79	0.80	0.81	0.66	0.76	0.66	0.69
A/NK	1.58	1.53	1.55	1.45	1.67	1.49	1.62	1.66
K_2O/Na_2O	2.69	3.06	2.79	3.19	1.79	3.40	2.50	1.87

Table 2. Trace element data of dioritic rock

	A16A	A19A	A22A	A30A	A34A	A35A	A36A	A39A	Average
Sc	25.00	21.00	21.00	18.00	28.00	22.00	25.00	22.00	22.75
V	153.00	176.00	171.00	170.00	165.00	191.00	159.00	173.00	169.75
Cr	616.00	233.00	227.00	218.00	487.00	298.00	573.00	451.00	387.88
Co	57.00	52.00	41.00	26.00	35.00	24.00	29.00	29.00	36.63
Ni	115.00	54.00	50.00	53.00	95.00	55.00	103.00	98.00	77.88
Cu	33.00	23.00	29.00	29.00	30.00	35.00	23.00	32.00	29.25
Zn	87.00	107.00	116.00	106.00	84.00	137.00	88.00	81.00	100.75
Ga	14.54	18.24	17.18	16.76	14.91	17.79	14.26	15.31	16.12
Rb	143.00	158.00	149.00	170.00	105.00	169.00	138.00	111.00	142.88
Sr	656.00	787.00	716.00	784.00	780.00	692.00	699.00	751.00	733.13
Y	34.00	39.00	37.00	37.00	32.00	40.00	33.00	31.00	35.39
Zr	446.00	857.00	762.00	744.00	521.00	863.00	399.00	549.00	642.63
Nb	25.00	40.00	36.00	37.30	24.70	45.50	19.80	23.50	31.48
Ba	1498.00	2141.00	2095.00	2235.00	1621.00	2148.00	1671.00	1813.00	1902.75
Th	13.62	23.82	17.11	19.35	11.99	21.62	15.94	14.15	17.20
U	2.23	3.67	3.34	3.35	2.63	3.52	2.13	2.72	2.95
	Rare earth elements								
La	78.00	101.00	73.00	78.00	48.00	87.00	60.00	55.00	72.50
Ce	160.00	209.00	172.00	175.00	109.00	196.00	122.00	119.00	157.75
Pr	18.50	23.40	20.70	22.30	14.20	25.70	14.80	14.70	19.288
Nd	73.50	93.40	84.00	83.00	54.00	99.00	55.00	55.00	74.613
Sm	73.50	15.90	15.40	15.10	9.90	18.20	9.50	9.50	20.875
Eu	12.20	2.90	2.91	3.59	2.19	4.11	2.21	2.25	4.045
Gd	2.22	11.45	10.60	13.00	8.61	15.80	8.25	8.29	9.778
Tb	1.28	1.65	1.57	1.68	1.10	2.16	1.05	1.04	1.441
Dy	7.66	9.54	9.51	8.35	5.77	12.60	5.49	5.39	8.039
Ho	1.39	1.77	1.82	1.62	1.12	3.00	1.07	1.06	1.606
Er	3.52	4.45	4.73	4.23	2.98	8.70	2.88	2.81	4.288
Tm	0.51	0.64	0.70	0.60	0.44	1.20	0.42	0.41	0.615
Yb	3.41	4.25	5.00	3.86	2.71	7.71	2.69	2.56	4.024
Lu	0.56	0.68	0.82	0.59	0.41	1.15	0.40	0.39	0.625
∑REE	470.25	519.03	439.76	447.92	292.43	522.33	318.76	308.40	414.860

REE: Rare Earth Element

Table 3. Representative ratios of trace elements

	A16A	A19A	A22A	A30A	A34A	A35A	A36A	A39A	Average
Rb/Sr	0.218	0.201	0.208	0.217	0.135	0.244	0.197	0.148	0.19
Ba/Rb	10.476	13.551	14.060	13.147	15.438	12.710	12.109	16.333	13.48
Ba/Sr	2.284	2.720	2.926	2.851	2.078	3.104	2.391	2.414	2.596
Th/U	6.108	6.490	5.123	5.776	4.559	6.142	7.484	5.202	5.860
K/Rb	278.075	303.691	309.221	301.788	314.67	295.714	276.72	311.123	298.875
K/Ba	26.545	22.412	21.992	22.955	20.383	23.266	22.853	19.048	22.432
$(Ce/Yb)_N$	14.401	15.094	10.558	13.915	12.345	7.803	13.920	14.267	12.788
$(Ho/Yb)_N$	0.119	0.121	0.106	0.122	0.120	0.113	0.116	0.121	0.117
$(La/Yb)_N$	15.457	16.059	9.866	13.655	11.969	7.625	15.072	14.518	13.028
$(La/Sm)_N$	6.466	6.425	4.794	5.224	4.904	4.835	6.388	5.855	5.611
$(Gd/Yb)_N$	2.129	2.183	1.718	2.729	2.575	1.661	2.486	2.624	2.263
Eu/Eu*	0.649	0.657	0.696	0.783	0.725	0.741	0.763	0.775	0.723

5. CONCLUSION

The sharp contact relationship between quartz-feldspathic gneiss, amphibolite and granitic rocks and occurrences of several generations of quartz-feldspar vein indicate the signature of *in situ* fractionation and different pulse of crystallization of fractionated magma. The presence of hornblende and biotite, and formation of secondary biotite after hornblende in the rocks of the study area are characteristics of "A" type granitoids. The K_2O/Al_2O_3 ratio is relatively low, which suggests derivation of magma by partial fusion of preexisting meta-igneous rocks. The lower value of A/CNK < 1 (avg. 0.73) and minimal amount of normative corundum (<1%) does not support sedimentary parentage of these rocks. The SiO_2 vs. Na_2O+ K_2O plot and SiO_2 vs. TiO_2 plot suggest igneous origin. The SiO_2 vs. A/CNK plot and the presence of hornblende, biotite and sphene are thus supporting the metaluminous character of these rocks. In geochemical plot, it is found that the rocks fall in monzonite to quartz monzonite field though the original rock are diorites. This is due to the increase of K_2O content as a result of K-metasomatism. The petrographic signature of the generation of secondary biotite and sphene at the border of biotite due to the expense of hornblende is a result of K-metasomatism in the rock.

Finally, it can be concluded that the petrographic and geochemical characters indicate that the dioritic rock of this area is having alkaline and metaluminous nature. Possibly these rocks are the product of recycled dehydration melting of lower crustal gabbroic rocks in within plate environment. After the culmination of crystallization and emplacement of dioritic body, it is affected by late phase K-metasomatism due to later emplacement of granitic rocks in the area. The crustal components are mixed with the hot magma during its emplacement towards the upper crust.

ACKNOWLEDGEMENTS

The authors are thankful to Dr. P.P. Khanna, former Head, Geochemistry Division, Wadia Institute of Himalayan Geology (WIHA), Dehradun for analytical support and Head, Department of Geological Sciences, Gauhati University for providing laboratory facilities.

COMPETING INTERESTS

Authors have declared that no competing interests exist.

REFERENCES

1. Bhagabaty B, Mazumdar MK, Mazumdar AC, Borah P. Geochemical characteristics of Tukureswari and Barbhita Granitoid in Goalpara District, Assam. Jour. Geol. Soc. India. 2017;89:532-540.
2. Mazumdar SK. A summary of the Precambrian geology of Khasi Hills, Meghalaya. Geol. Surv. India Misc. Publ. 1976;23(2):311-334.
3. Mazumdar SK. The Precambrian framework of part of the Khasi Hills, Meghalaya. Rec. Geol. Surv. India. 1986; 117:1-59.
4. Kumar S. Granitoids and their enclaves from east khasi hills of Meghalaya: Petrogenetic and geochemical reappraisal. Workshop on Geodynamics and natural Resources of North East India. Dibrugarh, Assam. Abstact volume. 1998:17–18.
5. Crawford AR. India, ceylon and Pakistan: New age data and comparison with Australia. Nature. 1969;223:80-84.
6. Chimote JS, Pandey BK, Bagchi AK, Basu AN, Gupta JN, Sarsawat AC. Rb-Sr whole-rock isochron age for theMyllium granite, Khasi Hills, Meghalaya. Fourth Natl. Symp. Mass spectrometry, Bangalore. 1988; 9(1-4).
7. Van Breeman O, Bowes DR, Bhattacharjee CC, Chowdhary PK. Late Proterozoic – Early Proterozoic Rb-Sr whole rock and mineral ages for granite and pegmatite, Goalpara, Assam, India, Jour. Geol. Soc. Ind. 1989;34(1):89–92.
8. Kumar S. Petrochemistry and geochronology of pink granite from Songsak, East Garo Hills, Meghalaya. Jour. Geol. Soc. India. 1990;35:27-279.
9. Selvam AP, Prasad RN, Raju RD, Sinha RM. Rb-Sr age of metaluminous granitoids of south Khasi batholiths, Meghalaya: implication on its genesis and Pan-African activity in North-Eastern India. Jour. Geol. Soc. India. 1995;46:619–624.
10. Ghosh S, Chakraborty S, Bhalla JK, Paul DK, Sarkar A, Bishui PK, Gupta SN. Geochronology and geochemistry of granite plutons from East Khasi Hills,

Meghalaya. Jour. Geol. Sci. India. 1991; 37:331-342.
11. Ghosh S, Chakraborty S, Paul DK, Bhalla JK, Bishui PK, Gupta SN. New Rb-Sr isotopic ages and geochemistry of granitoids from Meghalaya amd their significance in middle to late Proterozoic crustal evolution, Indian Minerals. 1994a; 48:33-44.
12. Ghosh S, Fallick AE, Paul DK, Potts PJ. Geochemistry and origin of Neoproterozoic granitoids of Meghalaya, Northeast India: Implications for linkage with amalgamation of Gondwana supercontinent. Gondwana Res. 2005;8:421-432.
13. Kumar S, Rino V, Hayasaka Y, kimura K, Shunmugan R, Terada K, Pathak M. Contribution of Columbia and Gondwana Supercontinent assembly- and growth-related magmatism in the evolution of the Meghalaya Plateau and the Mikir Hills, Northeast India: Constraints from U-Pb SHRIMP zircon geochronology and geochemistry. Lithos. 2017;277:356-375.
14. O`Connor JT. A classification of quartz rich igneous rock based on feldspar ratios. US Geological Survey. 1965;525B:B79-B84.
15. Middlemost EAK. Naming materials in the magma/ igneous rocks rock system. Earth Sci Rev. 1985;25:956-983.
16. MacDonald GA. Composition and Origin of Hawaii Lavas. Geological Society of America Memoirs. 1968;116:477-522.
17. Shand SJ. Eruptive rocks. Their genesis, composition, classification and their relation to ore-deposits with a chapter on Meteorites. John Wiley & Sons. New York. 1943.
18. Rollinson H. Using geochemical data: Evaluation, presentation, interpretation, Longman scientific & technical, New York. 1993;352.
19. Boynton WV. Cosmochemistry of the rare earth elements: Meteorites studies. In Henderson P. (ed), Rare earth element geochemistry. Amsterdam, Elsevier. 1984: 63-114.
20. Davis J, Hawkesworth CJ. Early calc-alkaline magmatism in the Mongollon-Dalil Volcanic field, New Mexico, USA. Jour Geol Soc London. 1994;151:825-843.
21. Thompson RN, Morrison MA, Hendry GL and Perry SJ. An assessment of the relative role of crust and mantle in magma genesis: An elemental approach. Phil. Trans. R. Soc. 1984;A310:549-590.
22. Turekian KK, Wedpohl KH. Distribution of elements in some major units of the Earth’s crust. Bull. Geol. Soc. Am. 1961; 72:175-192.
23. Pearce JA, Harris NBW, Tindle AG. Trace element discrimination diagrams for the tectonic interpretation of granitic rocks, Jour. Petrol. 1984;25(4):956–983.
24. Sadiq M, Umrao RK, Dtta JC. Occurrence of rare earth elements in parts of Nongpoh granite, Ri-Bhoi district, Meghalaya. Curr. Sci. 2014;106(20):162-165.
25. White R, Mackenzie D. Magmatism at Rift zones the generations of volcanic continental margins and flood basalts. Journal of Geophysical Research. 1989; 94:7685-7729.
26. Batchelor RA, Bowden P. Petrogenetic interpretation of granitic rock series using multicationic parameters. Chem. Geol. 1985;48:43-55.
27. Whalen JB, Currie KL, Chappel BW. A-type granites geochemical characteristics, discrimination and petrogenesis. Contrb. Miner. Petrol. 1987;95:407–419.

Peer-review history:
The peer review history for this paper can be accessed here:
http://www.sciencedomain.org/review-history/24417